Int. J. Heat Mass Transfer. Vol. 13, pp. 319–344. Pergamon Press 1970. Printed in Great Britain

TURBULENT AND LAMINAR HEAT TRANSFER TO GASES WITH VARYING PROPERTIES IN THE ENTRY REGION OF CIRCULAR DUCTS

C. A. BANKSTON
Los Alamos Scientific Laboratory, Los Alamos, New Mexico 87544

and

D. M. McELIGOT
Energy, Mass and Momentum Laboratory, Aerospace and Mechanical Engineering Dept., University of Arizona, Tucson, Arizona 85721

(*Received* 9 *November* 1968 *and in revised form* 11 *April* 1969)

Abstract—A numerical method is developed to solve the coupled boundary layer equations for turbulent flow of a gas with large property variations in a circular tube. Uniform and fully developed entering velocity profiles are treated. Axial variation of the heating rate is permitted and is used for comparison with experiments.

Cases treated include: (1) constant fluid properties, laminar flow with variation of hydrodynamic entrance length; (2) variable, idealized air properties with uniform laminar entering velocity profile; (3) constant properties, fully developed turbulent flow in the immediate thermal entry region; (4) constant fluid properties, turbulent flow, with uniform entering velocity profile; (5) variable, idealized air properties and real gas properties, turbulent flow at heating rates to $(q''_w/Gc_{p,i}T_i) = 0{\cdot}02$.

Predictions for several turbulent transport models are compared to an experiment with a peak wall temperature ratio (T_w/T_i) of about 12, and the model yielding the closest agreement in the thermal entry region, a version of van Driest's mixing-length model, is used for further predictions.

NOMENCLATURE

( ), fn( ), function of;
a, b, c, d, exponents for property variation, equation (1f);
A_{cs}, cross sectional area, $\pi D^2/4$;
A_j, B_j, C_j, D_j, coefficients in finite difference equations;
c, speed of sound;
c_p, specific heat at constant pressure;
D, diameter;
$\dot{E}$, enthalpy flow rate across specified surface;
g_c, dimensional constant, e.g. 32·17 ft-lbm/lbf-s^2;
G, average mass flux, $\dot{m}/A_{cs}$;
H, enthalpy; H_b, bulk enthalpy, $\dot{E}_{cs}/\dot{m}$;
h, convective heat transfer coefficient, $q''_w/(T_w - T_b)$;
k, thermal conductivity;
l, mixing length;
L, length; L_i, length of i-th control volume;
$\dot{m}$, mass flow rate;
p, pressure;
q, heat transfer rate across specified surface;
q''_w, heat flux from wall to gas;
r, radial coordinate; r_0, outer radius of control volume, r_i, inner radius;
T, absolute temperature;
u, gas velocity in axial direction;
v, gas velocity in radial direction;
V, gas bulk velocity, G/ρ_b;

x, axial coordinate; x_h, unheated length;
y, transverse coordinate, $r_w - r$.

Greek symbols

δ, approximate boundary layer thickness;
δ^*, displacement thickness, $r_w\{1 - \sqrt{[\dot{m}/(\pi\rho_c u_c)]}\}$;
ε, eddy diffusivity; ε_m, for momentum, ε_h, for heat;
κ, constant in turbulence models;
μ, viscosity;
ν, kinematic viscosity, μ/ρ;
ρ, density;
σ, weighing factor in finite difference equations;
τ, shear stress.

Non-dimensional parameters and variables

f, friction factor, $\tau_w/(G^2/g_c\rho_b)$; f_s, τ_w based on velocity gradient at wall; f_{app}, based on $\tau_{w,app}$, equation (14);
$\overline{H}$, enthalpy, $(H - H_i)/c_{p,i}T_i$;
l^+, mixing length, $l\sqrt{(\tau_w g_c/\rho)}/\nu$;
M, Mach number, V/c;
Nu, Nusselt number, hD/k;
$\bar{p}$, pressure deficit, $\rho_i g_c(p_i - p)/G^2$;
Pr, Prandtl number, $\mu c_p/k$;
q^+, wall heat flux parameter, $q''_w/(Gc_{p,i}T_i)$;
Q_i^+, wall heat flux parameter used for laminar flow, $q''_w r_w/k_i T_i$ or $q_i^+ Re_i Pr_i/2$;
$\bar{r}$, radial distance, r/r_w;
Re, Reynolds number, $4\dot{m}/(\pi D\mu)$;
u^+, axial velocity, $u\sqrt{(g_c\tau_w/\rho)}$;
x^+, axial distance, $x/(r_w RePr)$; x_i^+, evaluated at inlet properties, x_x^+, evaluated at local properties;
y^+, transverse distance, $y\sqrt{(g_c\tau_w/\rho)}/\nu$; y_l^+, constant in turbulence models, or laminar sublayer thickness;
$\bar{y}$, transverse distance, y/r_w.

Subscripts

app, apparent, equation (14);
b, evaluated at bulk temperature, $T(H_b, p)$;
c, center line;
cp, evaluated from prediction based on constant property idealization;
DB, modified Dittus–Boelter;
DKM, Drew, Koo and McAdams;
eff, effective, equation (8);
i, axial index; inner; evaluated at inlet properties;
j, radial index;
l, evaluated at edge of "laminar sublayer";
N, evaluated at node adjacent to wall;
r, in radial direction;
ref, reference value;
vD, van Driest;
w, evaluated at wall;
x, evaluated at local bulk properties at x;
y, evaluated at transverse position y;
∞, asymptotic value at large x.

Unless otherwise defined, an overscore indicates the variable has been normalized through division by its inlet value, e.g. $\bar{\rho} = \rho/\rho_i$.

FOR THE first time, the problem of turbulent flow at the thermal entrance of circular tubes is solved for gases with large variations in transport properties by simultaneously solving the coupled energy, x-momentum, and continuity equations. A numerical method is used. The present study (a) provides the means for studying various turbulence models that have been proposed, (b) develops a flexible program which should be useful in predicting wall temperatures and pressure drops for strongly heated, forced, internal flows, and (c) applies such predictions to problems of current interest.

Interest in the problem was stimulated by the severe heating conditions encountered in the coolant channels of solid-core nuclear rockets, and by the desire to study the rather unexpected experimental results of Perkins and Worsoe-Schmidt [1] and Taylor [2]. The approach developed is applicable to a broad class of low-speed, single-component convection problems, and its extension to high-speed compressible flows appears to be straightforward.

PREVIOUS WORK

The thermal entry region has been treated in the past rather completely under the specified conditions of constant fluid properties and of fully developed flow before heating is imposed [3–5]. With these solutions, axial variation of the wall heat flux may be handled by superposition since the energy equation is linear. Only flow in the process of axial transition from laminar to turbulent has not been discussed.

The problem of simultaneous development of temperature and velocity profiles for fluids with constant properties was first solved by Kays [6] for laminar flow by applying the hydrodynamic solution of Langhaar [7]. Comparable solutions of the partial differential governing equations for turbulent flow are unknown to the authors of this study; the entering flow, including possible laminar and transition regions, defies simple description and, lacking a description of the flow field, the energy equation cannot be solved.

The effect of property variation has been studied recently for laminar flow by finite difference methods [8–11]. Turbulent flow with strong property variation has been treated less completely. Diessler [12] developed an approximate method of solution by applying the integral energy equation, and Wolf [13] extended it slightly. However, in the limiting case of constant fluid properties, these analyses disagree with both the analytical solution [4] and accepted data [14]. To study whether the discrepancies were inherent in the method of solution rather than in the assumed velocity profile, Magee [15, 16] solved the energy equation in finite difference form. Essentially, he assumed Deissler's velocity profile and re-evaluated it at the local Reynolds number at each step. With properties almost constant at very low heating rates, Magee found good agreement. However, with the heating rate increased to give significant property variation, he found only slight improvement over Wolf's predictions. It is interesting to note that essentially only one turbulence model has been applied to internal flow with property variation—the one developed by Deissler [17]—but that over 20 have been studied for external compressible flow by Spalding and Chi alone [18].

Although many investigators have utilized finite difference methods for laminar flow phenomena, the direct solution of the corresponding approximate partial differential equations for turbulent flow has not been common. Recent developments in both digital computers and numerical methods now make this approach attractive, particularly when the flow can be adequately approximated by the boundary layer equations.

Conventional finite-difference approaches, explicit and implicit, were described quite well by Richtmyer [19] in 1957. He noted that implicit methods have usually been inherently stable and he presented an algorithm for the solution of the tridiagonal matrix which often results. Many numerical studies have applied Taylor's series expansions to the partial differential equations in order to derive finite-difference approximations [8, 11, 20]. With this method the truncation error can be reduced for a specified mesh size. However, Fromm [21] showed this method to be dangerous: one can set-up finite difference equations which fail to conserve energy (or some other conserved quantity).

The work of Patankar and Spalding [22] inspired the present effort. They developed a rapid, flexible, approximate procedure which involved an implicit method, with the difference equations formed to ensure conservation plus

stability in the solution of the set of equations at each axial step. These characteristics are carried into the present study. Several of their other features (e.g. elimination of iteration, approximate use of von Mises coordinates, and a Couette flow approximation at the wall) are not used in this investigation.

FORMULATION OF PROBLEM AND METHOD OF SOLUTION

Idealized problem

In the present study we assume that the fluid enters a circular tube with a specified temperature and velocity distribution. Heating of the fluid is initiated either at the entrance or at some point downstream and may vary arbitrarily with position. Body forces are neglected, and the Mach number is assumed to be small so that viscous dissipation and flow work terms may be omitted from the energy equation. No changes of phase or chemical composition occur within the tube.

The flow is assumed to be steady but may be either laminar or turbulent throughout. If it is turbulent, the transport properties are assumed to be represented by a sum of the molecular exchange coefficient and an eddy exchange coefficient for the turbulent motion as suggested by Boussinesq [23].

With these assumptions and the usual boundary layer approximations for internal flow, the governing equations* and their initial and boundary conditions are:

for continuity

$$\frac{\partial(\rho u)}{\partial x} + \frac{1}{r}\frac{\partial(\rho v r)}{\partial r} = 0, \tag{1a}$$

for x-momentum

$$\frac{1}{r}\frac{\partial}{\partial r}\left(\mu_{\text{eff}} r \frac{\partial u}{\partial r}\right) = \rho u \frac{\partial u}{\partial x} + \rho v \frac{\partial u}{\partial r} + g_c \frac{\mathrm{d}p}{\mathrm{d}x}, \tag{1b}$$

for energy

$$\frac{1}{r}\frac{\partial}{\partial r}\left(\frac{k_{\text{eff}}}{c_p} r \frac{\partial H}{\partial r}\right) = \rho u \frac{\partial H}{\partial x} + \rho v \frac{\partial H}{\partial r}, \tag{1c}$$

and integral continuity

$$\dot{m} = \int_{A_{cs}} \rho u \, \mathrm{d}A_{cs} \tag{1d}$$

with

$$\begin{aligned} u(0, r) &= u_i(r), \quad v(0, r) = v_i(r) \\ \rho(0, r) &= \rho_i(r), \quad H(0, r) = H_i(r) \end{aligned} \tag{1e}$$

and

$$u(x, r_w) = 0, \quad v(x, r_w) = 0$$

$$\frac{\partial u}{\partial r}(x, 0) = 0, \quad v(x, 0) = 0$$

$$\frac{\partial H}{\partial r}(x, 0) = 0, \quad \frac{k}{c_p}\frac{\partial H}{\partial r}(x, r_w) = q''_w(x). \tag{1f}$$

The relations between the properties are unspecified in developing the numerical procedure so they may be selected to suit particular problems. Three sets of property relations were used for various aspects of the present investigation: (1) constant properties, (2) power law approximations for low-pressure air properties of the form

$$\frac{\mu}{\mu_i} = \left(\frac{T}{T_i}\right)^a, \frac{k}{k_i} = \left(\frac{T}{T_i}\right)^b, \frac{c_p}{c_{p,i}} = \left(\frac{T}{T_i}\right)^d, \quad \frac{\rho}{\rho_i} = \left(\frac{T}{T_i}\right)^{-1} \tag{1g}$$

and (3) tabular properties for low-temperature gaseous nitrogen. The accuracy of the power law expressions depends on the temperature ranges over which they are applied. For example, $b = 0{\cdot}805$ describes the variation of thermal conductivity for nitrogen [24] within 3 per cent from 360 to 1800°R but only within 8 per cent from 180 to 2200°R.

* In equation (1b), g_c becomes unity when the S.I. unit system is observed but it is carried here for completeness.

*Numerical strategy**

In developing the present computer program conservation, simplicity, and stability are emphasized. The approximating finite-difference equations are derived from basic principles by setting up finite control volumes, applying the appropriate balances, and using simple approximations for the rate equations.

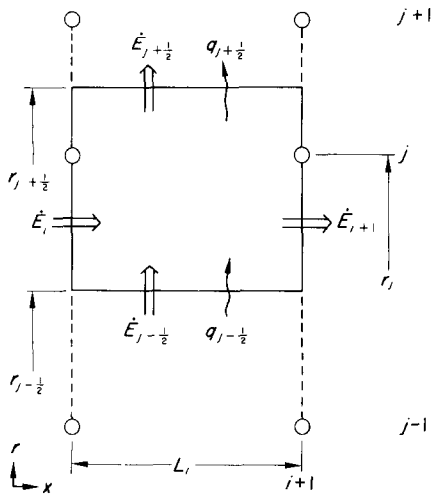

FIG. 1. Energy flows through surface of typical interior control volume.

Figure 1 demonstrates the relations between the control volumes and the mesh. The radial surfaces of each control volume are located halfway between adjacent mesh points. Radial locations of the nodes are adjusted so that mesh distances get successively smaller as the wall is approached; these locations are then kept fixed throughout the problem. Axial step size is primarily varied as the boundary layer thicknesses vary.

The procedure used to obtain the finite difference equations is essentially a rederivation of equations (1) for the macroscopic control volume. A few highlights are shown for the development of the finite difference equation for conservation of energy in order to demonstrate the essentials of the method.

* Details and a listing of the program are available in [25].

The energy flows considered for interior nodes are shown in Fig. 1 (at the boundaries the same method is used but some terms disappear). Conservation of energy requires*

$$\dot{E}_{i+1} + \dot{E}_{j+\frac{1}{2}} + q_{j+\frac{1}{2}} - \dot{E}_i - \dot{E}_{j-\frac{1}{2}} - q_{j-\frac{1}{2}} = 0. \tag{2}$$

Typical approximations of the rate equations for these flows are:

$$\dot{E}_{i+1} = \rho'_{i+1,j} u'_{i+1,j} \pi (r^2_{j+\frac{1}{2}} - r^2_{j-\frac{1}{2}}) [H_{i+1,j}] \tag{3a}$$

$$\dot{E}_{j+\frac{1}{2}} = \frac{\pi}{2} (\rho v)'_{j+\frac{1}{2}} r_{j+\frac{1}{2}} L_i (H_{i,j+1} + H_{i,j} + H'_{i+1,j+1} + H'_{i+1,j}) \tag{3b}$$

$$q_{j+\frac{1}{2}} = \frac{-2\pi r_{j+\frac{1}{2}} L_i}{r_{j+1} - r_j} \left(\frac{k_{\text{eff}}}{c_p}\right)_{i,j+\frac{1}{2}} \times \{(1-\sigma)(H_{i,j+1} - H_{i,j}) + \sigma([H_{i+1,j+1}] - [H_{i+1,j}])\}. \tag{3c}$$

In these rate equations the primed quantities represent predicted or estimated variables, the enthalpies in square brackets represent the unknowns, and the unmarked quantities represent those which have been calculated previously. The weighting factor, σ, provides control over the centering of the finite-difference representation with respect to the mesh.

The energy balance is formed with the rate equations such as equation (3), then the equation is non-dimensionalized and rearranged to the form

$$A_j [\bar{H}_{i+1,j+1}] + B_j [\bar{H}_{i+1,j}] + A_{j-1} [\bar{H}_{i+1,j-1}] + D_j = 0. \tag{4}$$

It may be seen that resulting equation (4) is linear. In a like manner, one may obtain the x-momentum equation†,

$$A_j [\bar{u}_{i+1,j+1}] + B_j [\bar{u}_{i+1,j}] + A_{j-1} [\bar{u}_{i+1,j-1}] + C_j \bar{p}_{i+1} + D_j = 0 \tag{5}$$

* Note that in equations (2)–(7) the subscript i denotes the index of the axial position in the finite difference mesh while in the remainder of the paper the subscript i refers to inlet conditions. Both notations are accepted standards and we hope their simultaneous use will not cause confusion.

† The values of coefficients A_j, B_j in the momentum equation differ from their counterparts in the energy equation.

the continuity equation,

$$\dot{m}_{r,j-\frac{1}{2}} = \dot{m}_{r,j+\frac{1}{2}} + (\bar{\rho}_{i+1,j}\bar{u}_{i+1,j} - \bar{\rho}_{i,j}\bar{u}_{i,j})(\bar{r}^2_{j+\frac{1}{2}} - \bar{r}^2_{j-\frac{1}{2}}) \quad (6)$$

and integral continuity equation,

$$\bar{\dot{m}} = \sum_{1}^{N+1} \bar{\rho}_{i+1,j}[\bar{u}_{i+1,j}](\bar{r}^2_{j+\frac{1}{2}} - \bar{r}^2_{j-\frac{1}{2}}) = 1. \quad (7)$$

The governing equations are solved sequentially at each step and are iterated until the solutions converge. The energy equation is solved for $\bar{H}(\bar{r})$ by applying the recurrence relations (essentially Gaussian elimination) presented by Richtmyer [19]. The x-momentum equation and the integral continuity equation are solved simultaneously for $\bar{u}(\bar{r})$ and $\bar{p}$ with the procedure described by Patankar and Spalding [22]. For the integral continuity equation, $\bar{\rho}(\bar{r})$ is calculated from $\bar{H}(\bar{r})$ found with the energy equation. Finally, the continuity equation is solved from the wall to the center to obtain $\bar{m}_r(\bar{r})$; the most recent values of $\bar{\rho}(\bar{r})$ and $\bar{u}(\bar{r})$ are used. Predicted values of the variables, necessary in the coefficients, are revised at each iteration. Once converged, the results for step $i + 1$ are taken for the first set of predicted values as the analysis moves to the next step.

Solution accuracy is obtained by successively refining the mesh to determine converged results for test cases. To conserve computer time, mesh parameters are chosen to give heat transfer and wall friction results within about 1 per cent of converged values. This level of accuracy is deemed adequate for the comparative purposes of the present paper. Usually 1 per cent accuracy was achieved with meshes containing 30–40 transverse mesh points and axial spacing of 2–5 boundary layer thicknesses. Computation time for such problems was typically less than 1 min of CDC 6600 time.

Turbulent model

While predictions for laminar internal flow with variable properties can be made with reasonable confidence once an adequate numerical method has been developed, there is not sufficient basic information for the comparable turbulent flows. Thus, the selection of a reasonable turbulent model must be one of the primary tasks of the present work.

The turbulent model is introduced in the program as a component of k_{eff} and μ_{eff},

$$\bar{\mu}_{\text{eff}} = \bar{\mu}\left(1 + \frac{\varepsilon_m}{\nu}\right) \quad (8)$$

$$\frac{\bar{k}_{\text{eff}}}{\bar{c}_p} = \frac{\bar{k}}{\bar{c}_p}\left(1 + Pr_i\frac{\bar{\mu}\bar{c}_p}{\bar{k}}\frac{\varepsilon_h}{\nu}\right). \quad (9)$$

As shown in equation (3c), these quantities are evaluated from the results of the preceding step with appropriate properties approximated on the radial control surface, i.e. at $r_{j+\frac{1}{2}}$, by interpolation. Reynolds' analogy, $\varepsilon_m = \varepsilon_h$, is assumed.

Models tested in the present investigation are listed in Table 1. With properties varying across the stream it is necessary to be specific in denoting the empirical form which is taken to be invariant in the model. For instance, if one choses a function $(\varepsilon/\nu) = \text{fn}(y^+)$, his results will differ in dependence on the properties upon which y^+ is defined; $y^+ = y\sqrt{(g_c\tau_w/\rho_w)}/\nu_w$ is numerically less than $y^+ = y\sqrt{[g_c\tau(y)/\rho(y)]}/\nu(y)$ when calculated at the same point in a heated gas flow. Thus, extensive subscribing is shown in Table 1 in order to denote explicitly the temperature at which the properties are to be calculated. The subscript "y" indicates the properties are evaluated at the temperature at y.

In the computer program $\varepsilon_{j+\frac{1}{2}}/\nu_{j+\frac{1}{2}}$ is derived from the basic representation of Table 1 for substitution in equations (8) and (9). For example, with the Reichardt "wall" model $\varepsilon_{j+\frac{1}{2}}/\nu_w$ is calculated from Table 1 then is multiplied by $\nu_w/\nu_{j+\frac{1}{2}}$ to obtain $\varepsilon_{j+\frac{1}{2}}/\nu_{j+\frac{1}{2}}$. Likewise, approximate piecewise integration is performed with the version entitled Kendall *et al.* "wall." In another paper [26], additional models were compared to heat transfer results for the downstream region of a strongly heated gas flow and it was concluded that the van Driest model

Table 1. Characteristics of turbulence models used

"Title"/Reference	Basic representation	κ	y_l^+	Range	Prediction for constant properties, $Re = 10^5$ Nu/Nu_{DB}	f/f_{DKM}	Identification in Fig. 2
Reichardt "wall" [30, 31]	$\frac{\varepsilon}{\nu_w} = \frac{\kappa}{6}\left[y_w^+ - y_l^+ \tanh\frac{y_w^+}{y_l^+}\right]\left[2 - \frac{y}{r_w}\right]\left[1 + 2\left(1 - \frac{y}{r_w}\right)^2\right]$	0·4225	11·0	Wall → ℄	0·945	0·989	R–w
Sparrow *et al.* "wall" [4]	$\varepsilon = n^2 uy\left[1 - \exp\left(-\frac{n^2 uy}{\mu/\rho}\right)\right]; n = 0{\cdot}124$ / $\frac{\varepsilon}{\nu_w} = \kappa y_w^+\left(1 - \frac{y}{r_w}\right) - 1$	0·36	26·0	$y_w^+ < y_l^+$ / $y_w^+ > y_l^+$	0·943	0·984	SHS–l
van Driest "local" [27]	$l = \kappa y\,[1 - \exp(-y_y^+/y_l^+)]$	0·4	Same	Wall → ℄	1·03	1·06	vD–l
van Driest "wall"	Same except replaced y_y^+ by y_w^+ in argument of exp	Same	Same	Same	Same	Same	vD–w
Kendall *et al.* "wall" [32]	$\frac{dl_y^+}{dy_y^+} = \frac{\kappa y_y^+}{y_l^+} - \frac{l_y^+}{y_l^+}\frac{\sqrt{(\tau_y/\rho_y)}}{\sqrt{(\tau_w/\rho_w)}}$	0·42	11·83	Wall → ℄	1·03	1·06	K w/o C–w
Kendall w/Clauser "wall" [32]	Wall region same form as Kendall *et al.* "wall" / Core (or wake): $\varepsilon + \nu = 0{\cdot}018\, u_c\delta^*$	0·44	11·83	$\varepsilon + \nu <$ $0{\cdot}018\,\mu_c\delta^*$	0·939	1·00	K w/C–w

[27], with the exponential term evaluated at the wall properties

$$l = 0{\cdot}4\, y\left[1 - \exp\left(-\frac{y\sqrt{(\tau_w g_c/\rho_w)}}{26\nu_w}\right)\right] \tag{10}$$

provided the best agreement. This version is transformed to $\varepsilon_{j+\frac{1}{2}}/\nu_{j+\frac{1}{2}}$ by relating the definitions of the mixing length and of the eddy diffusivity as

$$\varepsilon = l^2\left|\frac{du}{dy}\right| . \tag{11}$$

The velocity profile at the previous step is used in calculating the derivative.

Selection of turbulence model

During the last decade numerous experiments with turbulent flow and variable properties have been conducted to provide design correlations. Since the analyses mentioned above did not include a solution of the momentum equation, some of these experiments [1, 16, 28] provide the only information we have on friction factors under such conditions. Sources for experimental data were published by Perkins and Worsoe-Schmidt [1] in 1965 and by Taylor [29] in 1968; the reader is referred to these listings for further detail.

Data for an experiment with a strong heating rate are used as a test of the various suggested turbulence models under conditions of greatly varying properties across and along the tube. Run 140 from the studies of Perkins and Worsoe-Schmidt was chosen as one of the most severe experiments for which detailed data are available to the authors [1]. The magnitude and peculiar shape of their wall-temperature distribution provides a basis for eliminating several turbulent diffusivity models from further consideration. In the numerical predictions, power law properties for air ($a = 0{\cdot}67$, $b = 0{\cdot}805$, $d = 0{\cdot}095$) approximate the fluid property variation.

The comparison of the diffusivity models is striking. In Fig. 2, the wall temperatures predicted by the various models are compared to the measured temperatures. Also shown is the wall-temperature prediction obtained by applying a constant-properties correlation evaluated at the local properties,

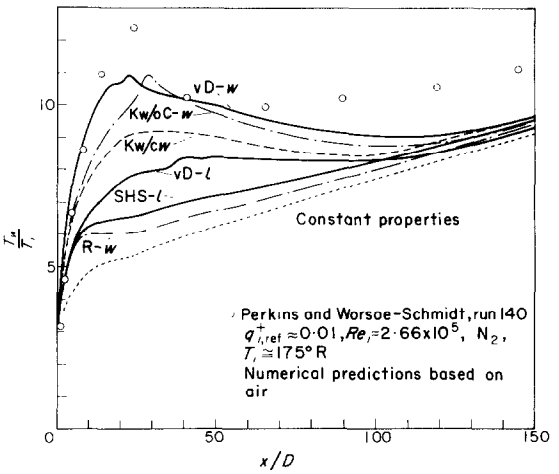

FIG. 2. Experimental data of Perkins and Worsoe-Schmidt [1]. Comparison to numerical predictions based on turbulent models listed in Table 1.

$$Nu = 0{\cdot}021\, Re_x^{0{\cdot}8} Pr_x^{0{\cdot}4}\left[1 + (x/D)^{-0{\cdot}7}\right] . \tag{12}$$

It is seen that the predictions which assume constant properties could lead to design of equipment in which overheating or failure might occur.

Two of the diffusivity models are superior to the others. The versions entitled "van Driest-wall" and "Kendall without Clauser-wall" [32] are closest to both the magnitude and the shape of the measured temperature distribution. Both predict approximately the same maximum temperature. However, because the results based on the van Driest description, equation (10), yield agreement with experimental data which is slightly better for the first 20 diameters and downstream, it is selected for prediction of additional results with property variation. In passing, it is noted that prediction with $\bar{v} \equiv 0$ leads to a peak wall temperature about 20 per cent lower than when $\bar{v}$ is included. Profile

Table 2. Comparison of Nusselt numbers for constant property, constant heat flux calculations

Laminar flow								Turbulent flow ($Re = 5 \times 10^4$)	
	Nusselt number							Nusselt number	
	Eigenvalue solution Ref. [3, 39]			Numerical solution		Series solution		Eigenvalue soln. Ref. [4]	Numerical solution
x^+	7 term	20 term	40 term	Std. grid	Converged	Ref. [33]	x/D	5 terms	Std. grid
0·001	15·068	15·336	15·839	15·843	15·80	15·813	0·1	172·8	225·0
0·0015	13·525	13·617	13·810	13·82	13·80	—	0·15	170·4	227·5
0·002	12·423	12·460	12·540	12·55	12·55	12·538	0·2	168·2	210·9
0·003	10·943	10·944	10·970	10·98	10·97	—	0·3	163·9	190·5
0·004	9·980	9·980	9·986	9·994	9·98	—	0·4	160·3	178·3
0·005	9·293	9·297	9·295	9·302	9·29	9·295	0·5	157·0	169·4
0·006	8·772	8·773	8·778	8·778	—	—	0·6	154·0	163·5
0·008	8·020	8·020	8·020	8·025	—	—	0·8	148·9	154·6
0·010	7·494	—	—	7·498	—	7·494	1·0	144·8	148·4
0·015	6·656	—	—	6·660	—	—	1·5	137·0	138·5
0·020	6·148	—	—	6·154	—	6·149	2·0	131·5	132·5
0·030	5·541	—	—	5·554	—	—	3·0	124·4	125·0
0·040	5·198	—	—	5·206	—	—	4·0	119·8	120·3
0·050	4·972	—	—	4·980	—	—	5·0	116·6	117·1
0·060	4·816	—	—	4·824	—	—	6·0	114·2	114·7
0·080	4·624	—	—	4·629	—	—	8·0	110·8	111·3
0·100	4·514	—	—	4·521	—	—	10·0	108·6	109·0
0·150	4·404	—	—	4·408	—	—	15·0	105·4	105·7
0·200	4·375	—	—	4·376	—	—	20·0	103·7	104·0
0·300	4·364	—	—	4·363	—	—	—	—	—
0·400	4·364	—	—	4·363	—	—	—	—	—
∞	4·364	—	—	4·363	—	—	∞	101·63	101·8

behavior and prediction based on tabulated properties for nitrogen, instead of on power laws for air, will be discussed in later sections.

LAMINAR-FLOW RESULTS

The main purpose of the laminar-flow calculations was to test the program in situations for which solutions were well known. However, new information was obtained for several cases and will be presented briefly.

Constant properties

Results are presented in Table 2 for a step change in wall heat flux after the velocity profile has become fully developed. In the downstream region agreement with the truncated eigenvalue solution of Siegel *et al.* [3] is encouraging, and additional confidence is gained by the comparison to the series solution of Worsoe-Schmidt [33] which is exact in the vicinity of the origin. For uniform entering flow profiles, results were obtained which were in close agreement with the pressure-drop predictions of Langhaar [7] and with the heat-transfer predictions of Hornbeck [34].

Heat-transfer experiments are often conducted in apparatus where heating begins after a short hydrodynamic entry section. Since up to 100 diameters may be necessary to establish a parabolic velocity profile, such experiments correspond to neither of the two common entry conditions in analysis: parabolic or uniform profiles. Accordingly, a number of calculations were conducted with various lengths for the unheated entrance section. The transverse velocity was taken to be zero at the flow entry. Heat-

transfer results are compared to the present predictions for the parabolic entering profile in Fig. 3. In this figure x_h refers to the unheated length. As expected, the Nusselt numbers become higher as the unheated entry is reduced,

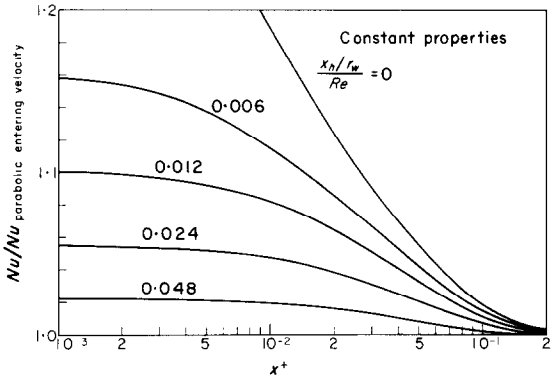

FIG. 3. Effect of insufficient flow development length on laminar heat transfer.

eventually approaching the results for a uniform entering velocity profile. Of particular interest to the experimentalist is the hydrodynamic entry necessary to obtain fairly close agreement with the predictions based on fully developed flow at the thermal entrance. With only one-tenth of a hydraulic entrance distance the heat-transfer predictions agree within 10 per cent for $x^+ > 0{\cdot}001$.

Air properties, fully developed entering flow

The present calculations are in close agreement with the variable properties, numerical analysis of Worsoe-Schmidt [8, 9]. His correlation for heat transfer is found within 7 per cent of the present results for $Gz_x \geqslant 3$ up to a heating rate of $Q_i^+ = 50$* (Table 3). Further, his observations of velocity maxima displaced from the tube axis are also confirmed.

Regarding prediction of wall friction, Worsoe-Schmidt notes a possible discrepancy between his results and experimental data. His correlation is

$$(f \cdot Re_x/16) = (T_w/T_b)^1 \qquad (13)$$

* Our Q_i^+ corresponds to Worsoe-Schmidt's q^+.

while recent data lead to an exponent greater than unity for the temperature ratio. In passing, he indicates a difference between his definition of f and that employed in data reduction.

Measured friction factors, such as those presented by Davenport and Leppert [35], are based on the "apparent wall shear stress" calculated from a one-dimensional force balance which includes the axial momentum change as follows

$$\tau_{w,\mathrm{app}} = -\frac{D}{4}\frac{\mathrm{d}}{\mathrm{d}x}\left\{p + \frac{G^2}{\rho_b g_c}\right\}. \qquad (14)$$

One-dimensional design predictions also employ equation (14) as a basis. On the other hand, analytical predictions determine τ_w from $(\partial u/\partial y)_w$. The two methods are numerically equivalent only when the axial momentum gradient is the same regardless whether calculated from one-dimensional parameters or from the profiles; this situation occurs when $\partial u/\partial x$ is zero as in fully developed flow, but a heated gas develops continually.

The friction factors defined from the two different evaluations of the wall shear stress are

$$f_{\mathrm{app}} = \frac{\tau_{w,\mathrm{app}}}{G^2/(2\rho_b g_c)} \text{ and } f_s = \frac{\mu_w(\partial u/\partial y)_w}{G^2/(2\rho_b g_c)} \qquad (15)$$

respectively. Figure 4 presents the difference between the two at a high heating rate. It is seen that f_{app} is greater than f_s. While the maximum difference is only about 15 per cent at $(T_w/T_b) \approx 2$, the difference in the exponents on the temperature ratio is about 0·25. Thus, it appears that the numerical results of Worsoe-Schmidt and Leppert [8] and the data of Davenport and Leppert are not actually in serious disagreement.

Air properties, uniform entering profile

In the process industries, most heating equipment lacks the unheated entrance which was included in the previous section. A uniform entering profile is a better idealization for such equipment than the parabolic profile. For this idealization, effects of gas-property variation are presented for one heating rate each by

Table 3. Parabolic entering velocity profile, power law air properties, $Q_i^+ = 50$ (constant)

x_i^+	x_x^+	T_b/T_i	T_w/T_b	Nu	$\frac{f_{app} \cdot Re_x}{16}$	$\frac{f_s \cdot Re_x}{16}$
0·001	0·00114	1·198	4·335	21·63	5·385	5·155
0·0015	0·00180	1·296	4·388	18·48	5·325	5·273
0·002	0·00253	1·393	4·357	16·37	5·262	5·249
0·003	0·00416	1·586	4·201	13·59	5·103	5·045
0·004	0·00601	1·776	4·011	11·77	4·899	4·773
0·005	0·00808	1·965	3·821	10·48	4·705	4·509
0·006	0·0103	2·152	3·642	9·493	4·524	4·263
0·008	0·0154	2·521	3·328	8·098	4·170	3·838
0·01	0·0212	2·885	3·067	7·150	3·867	3·495
0·015	0·0385	3·777	2·569	5·754	3·271	2·892
0·02	0·0596	4·649	2·247	5·007	2·871	2·496
0·03	0·111	6·351	1·825	4·307	2·302	2·000
0·04	0·175	8·01	1·570	4·101	1·905	1·686
0·05	0·250	9·636	1·407	4·115	1·619	1·468
0·06	0·334	11·24	1·305	4·168	1·426	1·324
0·08	0·531	14·38	1·192	4·229	1·234	1·182

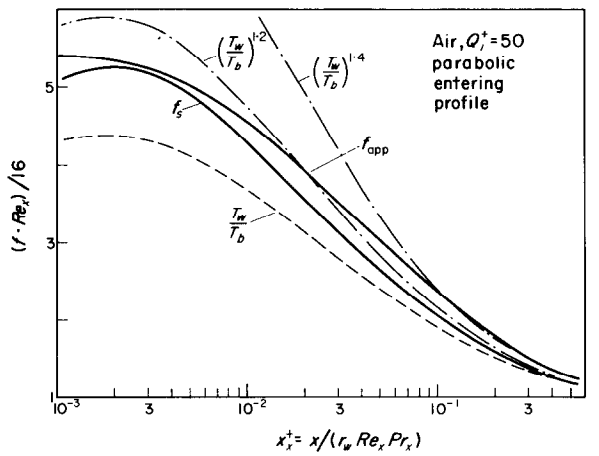

FIG. 4. Comparison of experimentalist's definition of friction factor, f_{app}, and usual definition in analysis, f_s. Strong heating of laminar flow.

Deissler and Presler [11] and by Worsoe-Schmidt [36]. They show that the change in Nusselt number is slight, compared to results without property variation if both are evaluated at local conditions, but friction parameters may be tripled.

More extensive results are presented for Q_i^+ from 0 to 30 in Table 4. In general, trends are the same as shown by Worsoe-Schmidt with fully developed initial flow, although the effect of high heating rates on friction parameters is somewhat obscured by the usual strong entry variation. Again the location of the peak temperature ratio, $(T_w/T_b)_{max}$, moves closer to the entrance as the heating rate is increased. And use of x_x^+ provides a closer grouping of the

Table 4. Wall parameters for laminar flow of air. Uniform entering velocity profile, constant wall heat flux

x_i^+	x_x^+	T_b/T_i	T_w/T_b	Nu	$\frac{p_i - p}{G^2/\rho_i g_c}$	$f_{app} \cdot Re_x$	$f_s \cdot Re_x$
			$Q_i^+ = 0$ (constant properties)				
0·001	0·001	—	—	24·18	0·1237	95·88	50·08
0·002	0·002	—	—	17·62	0·1776	68·17	39·05
0·005	0·005	—	—	11·83	0·2881	44·63	29·18
0·01	0·01	—	—	8·936	0·4196	33·37	24·18
0·02	0·02	—	—	6·928	0·6204	25·77	20·66
0·05	0·05	—	—	5·267	1·079	19·58	17·70
0·1	0·1	—	—	4·617	1·710	17·06	16·48
0·2	0·2	—	—	4·385	2·859	16·12	16·05
0·5	0·5	—	—	4·363	6·226	16·01	15·98
			$Q_i^+ = 0{\cdot}3$				
0·001	0·001001	1·001	1·025	24·18	0·1262	97·56	50·47
0·002	0·002003	1·002	1·034	17·63	0·1826	69·81	39·56
0·005	0·005021	1·006	1·050	11·85	0·3008	46·22	29·90
0·01	0·01009	1·012	1·066	8·950	0·4460	34·97	25·09
0·02	0·02034	1·024	1·083	6·935	0·6768	27·45	21·79
0·05	0·05211	1·060	1·103	5·252	1·243	21·40	19·11
0·1	0·1083	1·119	1·107	4·585	2·106	18·92	17·98
0·2	0·2327	1·237	1·094	4·335	3·903	17·80	17·40
0·5	0·6937	1·586	1·060	4·323	10·77	17·02	17·86
			$Q_i^+ = 1$				
0·001	0·001003	1·004	1·082	24·20	0·1319	101·54	51·43
0·002	0·002011	1·008	1·112	17·65	0·1941	73·32	40·73
0·005	0·005071	1·020	1·162	11·88	0·3300	49·60	31·54
0·01	0·01028	1·040	1·208	8·973	0·5062	38·27	27·13
0·02	0·02112	1·080	1·251	6·933	0·8055	30·72	24·18
0·05	0·05685	1·198	1·278	5·192	1·622	24·47	21·63
0·1	0·1266	1·393	1·244	4·497	3·041	21·41	20·03
0·2	0·3007	1·776	1·165	4·308	6·464	19·15	18·48
0·5	1·061	2·885	1·069	4·306	23·23	17·13	17·00
			$Q_i^+ = 2$				
0·001	0·001006	1·008	1·163	24·23	0·1399	106·7	52·77
0·002	0·002023	1·016	1·220	17·69	0·2102	78·00	42·42
0·005	0·005141	1·040	1·313	11·92	0·3704	53·77	33·81
0·01	0·01056	1·080	1·388	8·988	0·5895	42·09	29·81
0·02	0·02221	1·159	1·444	6·903	0·9841	34·19	27·05
0·05	0·06328	1·393	1·432	5·091	2·161	27·20	23·99
0·1	0·1504	1·776	1·323	4·393	4·413	22·88	21·29
0·2	0·3856	2·521	1·175	4·297	10·40	19·41	18·67
0·5	1·489	4·649	1·058	4·300	44·62	16·87	16·85
			$Q_i^+ = 5$				
0·001	0·001014	1·020	1·395	24·40	0·1604	118·4	56·37
0·002	0·002056	1·040	1·521	17·87	0·2535	88·81	47·20
0·005	0·005349	1·100	1·701	12·03	0·4830	62·82	39·94
0·01	0·11137	1·198	2·160	8·896	0·8246	49·91	36·37
0·02	0·02531	1·393	1·813	6·756	1·499	40·54	32·90
0·05	0·08077	1·965	1·613	4·820	3·792	30·42	26·96

Table 4.—(cont.)

x_i^+	x_x^+	T_b/T_i	T_w/T_b	Nu	$\frac{p_i - p}{G^2/\rho_i g_c}$	$f_{app} \cdot Re_x$	$f_s \cdot Re_x$
0·1	0·2122	2·885	1·349	4·240	8·780	23·45	21·76
0·2	0·5955	4·649	1·147	4·258	23·80	18·70	18·06
0·5	2·498	9·636	1·039	4·329	128·5	16·68	16·50
				$Q_i^+ = 10$			
0·001	0·001028	1·040	1·765	24·36	0·2000	136·6	63·10
0·002	0·002112	1·080	1·973	17·90	0·3275	102·2	55·16
0·005	0·005685	1·198	2·204	11·98	0·6610	71·75	48·58
0·01	0·01266	1·393	2·250	8·794	1·195	56·65	43·90
0·02	0·03007	1·776	2·105	6·418	2·332	45·00	37·82
0·05	0·1061	2·885	1·655	4·510	6·618	31·39	27·87
0·1	0·2977	4·649	1·297	4·210	16·70	22·30	20·92
0·02	0·8762	8·010	1·108	4·313	50·07	18·04	17·65
0·05	3·808	17·45	1·027	4·309	315·9	16·26	16·39
				$Q_i^+ = 30$			
0·001	0·001083	1·119	2·984	24·68	0·3278	167·9	86·82
0·002	0·002327	1·237	3·265	18·03	0·5721	120·6	79·70
0·005	0·006937	1·586	3·262	11·54	1·280	82·77	67·62
0·01	0·01723	2·152	2·889	7·967	2·560	63·68	54·83
0·02	0·04612	3·244	2·296	5·532	5·649	47·43	41·03
0·05	0·1858	6·351	1·515	4·141	19·01	28·52	25·56
0·1	0·5571	11·24	1·178	4·289	53·79	19·56	18·81
0·2	1·706	20·48	1·060	4·285	191·9	16·82	16·90
0·5	7·616	46·33	1·014	4·322	1482	16·06	16·19

Nusselt-number curves than x_i^+; when evaluated at the same value of x_x^+ the maximum difference between Nusselt numbers for $Q_i^+ = 0$ and $Q^+ = 30$ is only about 10 per cent.

The effect of heating on friction parameters is demonstrated in Fig. 5. Heating increases both $f_{app} \cdot Re_x$ and $f_s \cdot Re_x$. In contrast to the heat-transfer behavior, there appears to be no advantage to basing the abscissa, x^+, on the local Peclet number; the curves would merely be spread further apart. When the constant-property result ($Q^+ = 0$) is taken as a reference, it is seen that the local location of the maximum difference in $f_{app} \cdot Re_x$ moves closer to the entrance as the heating rate is increased. This observation leads to the suggestion that the behavior might be approximately correlated as a function of temperature ratio, as in the case with the parabolic entering profile. The suggestion may be examined with the aid of the insert in Fig. 5. For the ordinate, the product of apparent friction factor and local Reynolds number has been normalized by the product for constant properties, evaluated at the same value of x_i^+. Arrows on the paths represent the direction of increasing axial position; each curve starts at $x_i^+ = 0{\cdot}001$. It appears that some distance beyond the location of the peak temperature ratio the curves approximately approach an asymptotic behavior with a slope of the order of unity. At shorter distances the curves are comparable to one another in shape, but do not correspond to a simple function of the temperature ratio. However, for the lower heating rates or far downstream, the designer may find the approximation

$$\left[\frac{(f_{app} \cdot Re_x)}{(f_{app} \cdot Re)_{cp}}\right]_{x_i^+} \approx \left(\frac{T_w}{T_b}\right)^{0.9} \tag{16}$$

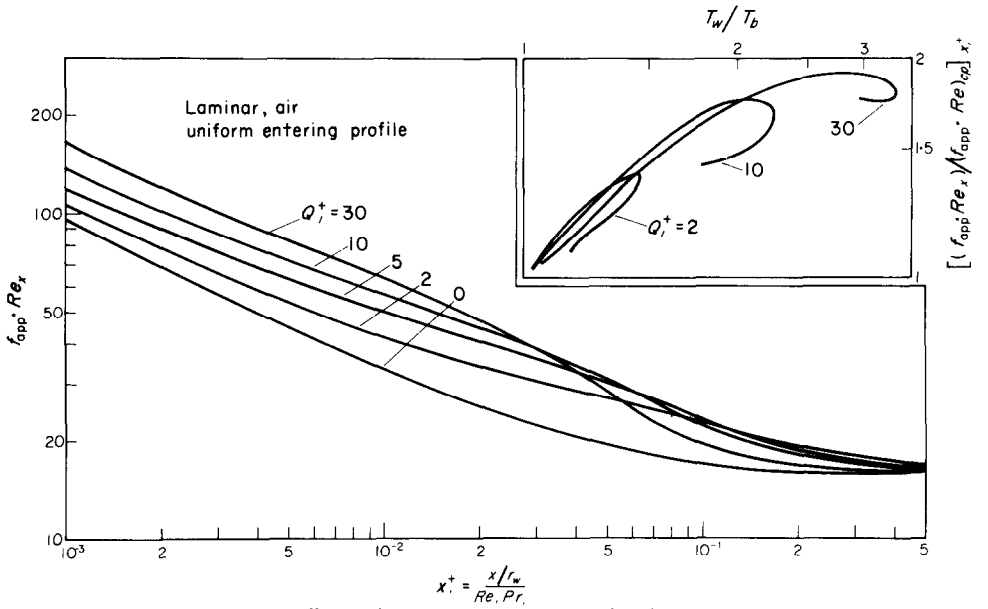

FIG. 5. Effect of heating on apparent friction factor in the entrance of a tube. Simultaneous development of boundary layers.

to be sufficiently accurate for his purposes. This relation predicts friction factors within ± 10 per cent for the entire curve at $Q^+ = 2$ and for downstream temperature ratios less than 1·8 at the higher heating rates. Equation (13) would be conservative in the sense that the pressure drop would be over-predicted if applied throughout the tube for the higher heating rates.

TURBULENT-FLOW PREDUCTIONS

Constant properties, fully developed entering flow

Present results for the Graetz problem with turbulent flow and with constant wall heat flux are compared in Table 2 to the eigenvalue solution of Sparrow *et al.* [4]. Numerical values shown are based on the eddy diffusivity model specified by the latter authors. It is seen that the two solutions agree to within 0·5 per cent after $x/D = 3$. Below this value, the present solution is preferred to the five-term eigenvalue solution. With only five terms, the normalized Nusselt number, Nu/Nu_∞, approaches a value of the order of 2 as x is reduced to zero, instead of approaching infinity as it should.

The Nusselt number variation in the immediate vicinity of $x = 0$ can be predicted by a Leveque type solution [33]. For a constant wall heat flux, the first order approximation (linear profile) leads to

$$Nu = \left[1{\cdot}935\left(\frac{x/D}{Re^2 Prf}\right)^{\frac{1}{3}} - \frac{4x/D}{RePr}\right]^{-1}. \quad (17)$$

It is expected that this relation will give a reasonable prediction for turbulent flow while the thermal boundary layer remains within the transverse range for which $u^+ \approx y^+$. Thus, it should describe the limiting behavior for the Nusselt number as x approaches zero. If the bulk temperature rise is neglected and Blasius and modified Dittus–Boelter correlations are used, it may be seen that dependence of the normalized Nusselt number on Reynolds number is slight:

$$\frac{Nu}{Nu_\infty} = 10{\cdot}56\, Re^{-0{\cdot}218}\, Pr^{-0{\cdot}067}\, (x/D)^{-\frac{1}{3}}. \quad (18)$$

The present numerical predictions may be shown to converge to the proper initial asymptotic behavior in the range $0{\cdot}001 \lesssim x/D \lesssim 0{\cdot}01$ after the first few axial steps.

If the results are to be useful for problems involving axial variation of the wall heat flux without rerunning the program for each case, a simple correlation must be developed. Unfortunately, a convenient one was not found which would approach asymptotes at both large and small x and still represent the intermediate results closely. Therefore, the requirement on the asymptotic behavior was relaxed to the specifications that $Nu \to \infty$ as $x \to 0$ and that the magnitude agreed with the numerical results to some "reasonably" small axial distance. For the van Driest mixing length model, the following correlation was obtained graphically for Reynolds numbers of 5×10^4, 1×10^5, 2×10^5 and 5×10^5.

$$\frac{Nu}{Nu_\infty} = 1 + 2{\cdot}20\, Re^{-0{\cdot}144}(x/D)^{-0{\cdot}807 Re^{-0{\cdot}0516}} \times \exp\{-1{\cdot}42\, Re^{-0{\cdot}20}(x/D)\} \qquad (19)$$

This relation conforms to the numerical results within 2 per cent for $x/D > 0{\cdot}1$. The Nusselt number for fully developed flow may be approximated as

$$Nu_\infty = 0{\cdot}0259\, Re^{0{\cdot}785}\, Pr^{0{\cdot}4} \qquad (20)$$

over the same range of Reynolds numbers. These fully-developed Nusselt numbers are slightly higher than those predicted with the diffusivity specified by Sparrow *et al.* [4]. One might say that the diffusivity is effectively higher at the same Reynolds number. Consequently, the thermal boundary layer spreads into the core more rapidly and the normalized Nusselt number, Nu/Nu_∞, is 5–8 per cent less for $0{\cdot}1 < x/D < 10$ (at $Re = 10^5$). Since $Nu_{\infty,vD}$ is larger, the resulting predictions of wall temperature would be close in this region.

Main advantages of the present correlation are (1) a close fit to the theoretical results at shorter axial distances than with the available five-term eigenvalue solution, and (2) continuous dependence on Reynolds number instead of individual tabulations at separate Reynolds numbers.

Constant properties, uniform entering flow

Predictions of the flow field in the hydrodynamic entry region were made using the eddy diffusivity models of van Driest, of Kendall *et al.*, of Reichardt and of Sparrow *et al.* These predictions were carried out at the conditions of the experiments of Barbin and Jones [37] who took great care to see that their experiments were close to the idealizations of most theoretical analyses as possible. They found that the velocities, intensities of turbulence, and Reynolds stresses were still changing at 43·5 diameters. However, the wall shear stress had obtained its fully developed value within some 15 diameters.

Unlike the experiments, all the numerical predictions demonstrated a fully-developed axial velocity profile in less than 40 diameters. The profiles from the diffusivity models investigated closely resemble the data, except near the axis where the experimental results exhibit a wake region similar to that observed in external boundary layers. The axial development of the velocity profiles predicted with the van Driest mixing length is likewise in concert with the findings of Barbin and Jones.

The development of wall shear stress is shown in Fig. 6, and here the predictions based on the van Driest mixing length are in strikingly good agreement with experiment. The entry length of 12·5 diameters is essentially identical to that found experimentally. By way of comparison, we find that the geometrical type of eddy diffusivity models yield shear stresses which develop more slowly than experiment, while the Kendall model employing the Clauser assumption develops shear stresses somewhat more rapidly. A modification of the Reichardt model in which the diffusivity was calculated using the boundary layer thickness (i.e. y/δ in place of y/r_w) is in better accord with experiments than when y/r_w is used.

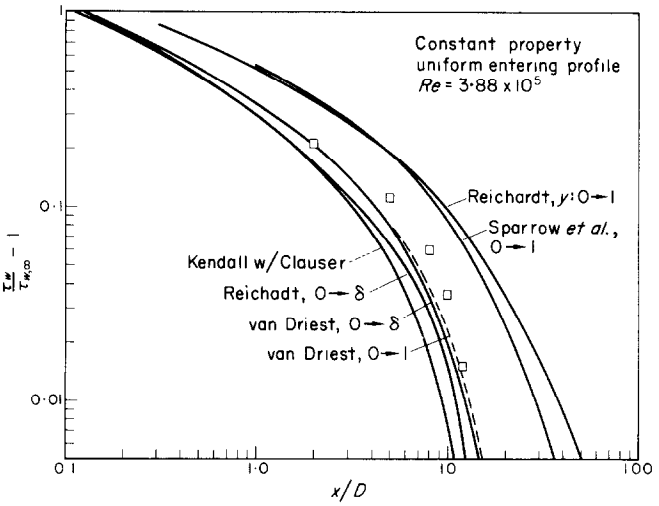

FIG. 6. Comparison of calculated shear stress distributions in hydrodynamic entry and data of Barbin and Jones [37].

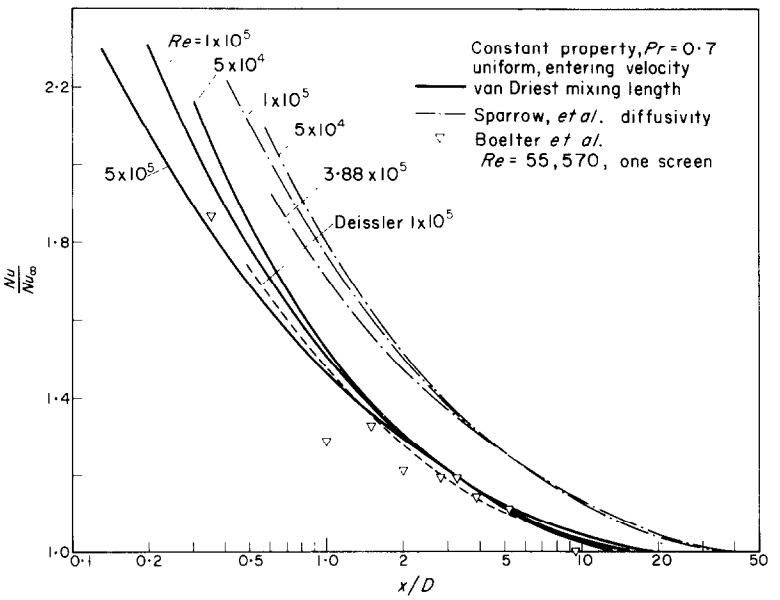

FIG. 7. Comparison of heat transfer solutions for simultaneous development of velocity and temperature profiles in turbulent entry flow. Present predictions compared to integral boundary layer method of Deissler [12] and data of Boelter *et al.* [38].

The constant-property heat-transfer results for simultaneous development of temperature and velocity profiles are shown in Fig. 7, with entering Reynolds numbers of 50000, 100000 and 500000. Predictions are shown for the van Driest and the Sparrow *et al.* diffusivity models. The heat-transfer results are consistent with the shear stress results described above, in that the Nusselt numbers obtained with the geometrical type of diffusivity tend to develop more slowly

than the mixing-length type. For comparison, the results of the Deissler integral analysis [12] for $Re = 100\,000$ is shown and it agrees quite well with the van Driest calculation. A single set of experimental points from the experiments of Boelter *et al.* [38] is also shown. The experimental data were taken at a Reynolds number of 55 570 with a bellmouth and a single screen at the entrance.

Air properties, fully developed entering flow

The treatment of turbulent flow with strong variation of fluid properties is one of the major goals of this work. This section presents the results of a series of calculations for entering Reynolds numbers from 5×10^4 to 5×10^5 and constant heating rates from $q^+ = 0{\cdot}001$ to $0{\cdot}02$. The latter run led to a peak wall-to-bulk temperature ratio of about 16 and is therefore chosen for further emphasis. Power laws describe the property variation.

at the same local bulk Reynolds number. For the constant-properties predictions, which are included for comparison, $Nu_{cp,x}$ then is simply Nu_∞. At small axial distances the results for the same entering Reynolds number seem to converge. As with the constant-property results, discussed earlier, the normalized Nusselt number increases as the entering Reynolds number is reduced. As x increases, the curves pass through minima and then increase as the temperature ratios decrease towards unity. The minima become lower as q^+ and Re are increased. As in the laminar results, the peak temperature ratio moves towards the entry as the heating rate is increased; the minimum normalized Nusselt number likewise moves forward, but it lags the peak temperature ratio.

Resulting wall-temperature distributions are shown in Fig. 9 for several heating rates. They increase as q^+ increases at a given Reynolds number, as expected. But the shapes vary. The

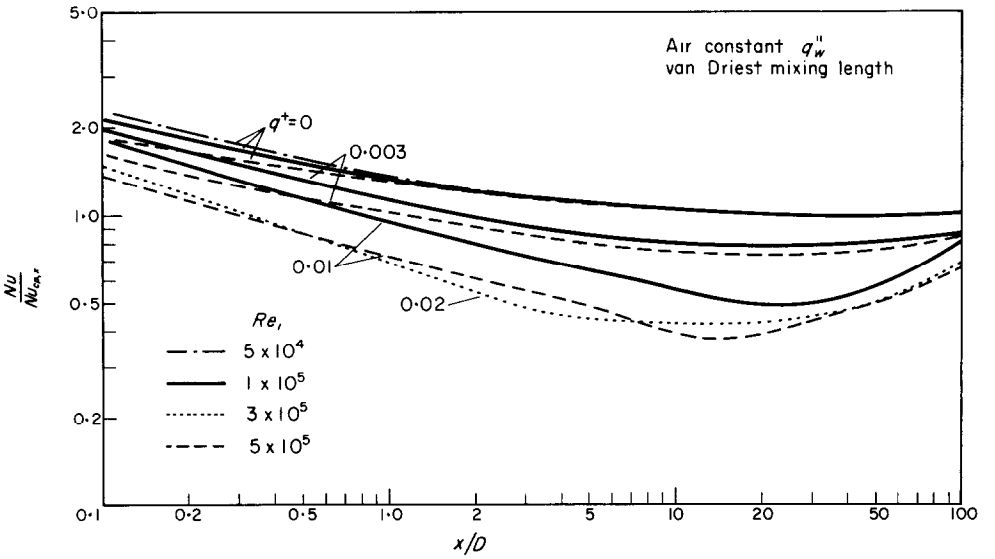

FIG. 8. Heat transfer predictions with property variation included. Fully developed entering velocity profile.

Heat-transfer results are presented in Fig. 8 for several runs. The ordinate is the Nusselt number divided by $Nu_{cp,x}$, the fully-developed Nusselt number which would be predicted by the constant-properties idealizations if evaluated

lowest heating rate shows a distribution typically described as increasing in the entry region towards an asymptote which is parallel to the bulk temperature rise [39]. At $q^+ = 0{\cdot}003$ a slight hump appears in the first 30 diameters,

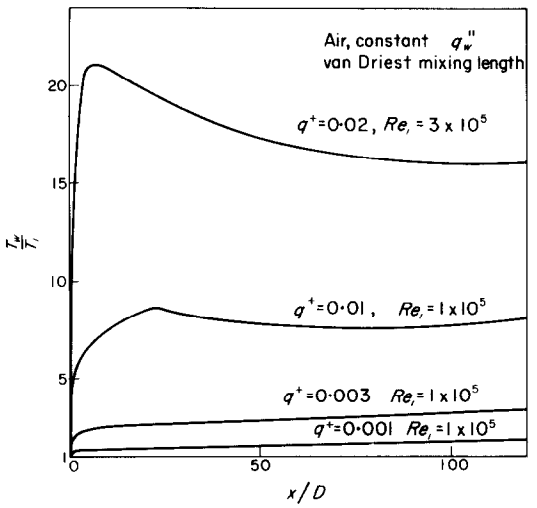

FIG. 9. Wall temperature predictions for turbulent flow with property variation. Fully developed entering velocity profile.

but the distribution increases monotonically and, in general, is comparable to the curve for $q^+ = 0{\cdot}001$. For the two higher heating rates shown, maximum wall temperatures appear in the thermal entrance. At the highest rate the peak is about 25 per cent higher than downstream; it should serve as a warning that downstream instrumentation may not be adequate protection in high-power applications.

Meaningful presentation of the velocity profiles becomes more difficult as the heating rate is increased. In Fig. 10(a) profiles for a moderate heating rate are compared at several axial stations with the profile in the unheated entrance region; standard semilogarithmic $u_w^+ - y_w^+$ coordinates are used. The most obvious effect is a reduction in magnitudes which is caused by the increased wall viscosity used in the definition of these variables. In general, the shapes remain comparable to the entering profile, though T_w/T_b is greater than 2. It appears that the profiles depart from the $u^+ = y^+$ behavior of the viscous wall layer at slightly higher values of y_w^+ than for the adiabatic entering profile. And since y_w^+ is already foreshortened by the increased wall viscosity, it becomes apparent that heating causes the thickening of the viscous layer (in terms of the physical distance, y/r_w). The thicker viscous layer implies less turbulent transport of energy, so local resistance to heat transfer is increased and the Nusselt number is decreased, as already noted. The heating condition described is typical of experiments with air entering at room temperature and is somewhat more severe than current practice for gas-cooled nuclear reactors in central power stations.

The velocity effects at the most extreme heating condition studied are not as clear. The standard presentation appears in Fig. 10(b). The temperature ratios up to 16 lead to a greater shrinking of the coordinates. The shapes are not comparable to the entering profile until well downstream where the temperature ratio is again modest; the use of integral boundary layer analyses with $u^+ - y^+$ similarity is therefore not justified for strongly heated thermal entries. For the first three heated profiles shown, the divergence from $u^+ = y^+$ seems to begin at smaller values of y_w^+ than for adiabatic flow. Therefore, specification of constant y_l^+ or u_l^+ as a criterion for viscous sublayer thickness appears meaningless for these highly heated conditions. From the standard plot one cannot determine whether the viscous layer has thickned or not. An indicator which retains significance would be the locus of a specified level of the turbulence Reynolds number, or non-dimensional eddy diffusivity, ε/ν. Small values correspond to predominantly viscous behavior while turbulent fluctuations are more important when $(\varepsilon/\nu) \gg 1$. The first locus where the effects are approximately equally important (i.e. $\varepsilon = \nu$) is plotted in Fig. 11 for the results shown in Fig. 10(b). Also, the comparable curves that would exist for an adiabatic profile at the same Re_x is indicated by a dashed line. In this figure, a thickening of the viscous layer by over 20 times is evident. It appears near the axial location of the peak in the temperature ratio ($x/D \sim 3$). The usual consequences follow: The Nusselt number is reduced severely and wall temperatures soar.

The results for strong heating show that maximum velocity occurs near the wall in some axial regions. The same effect was noted in the

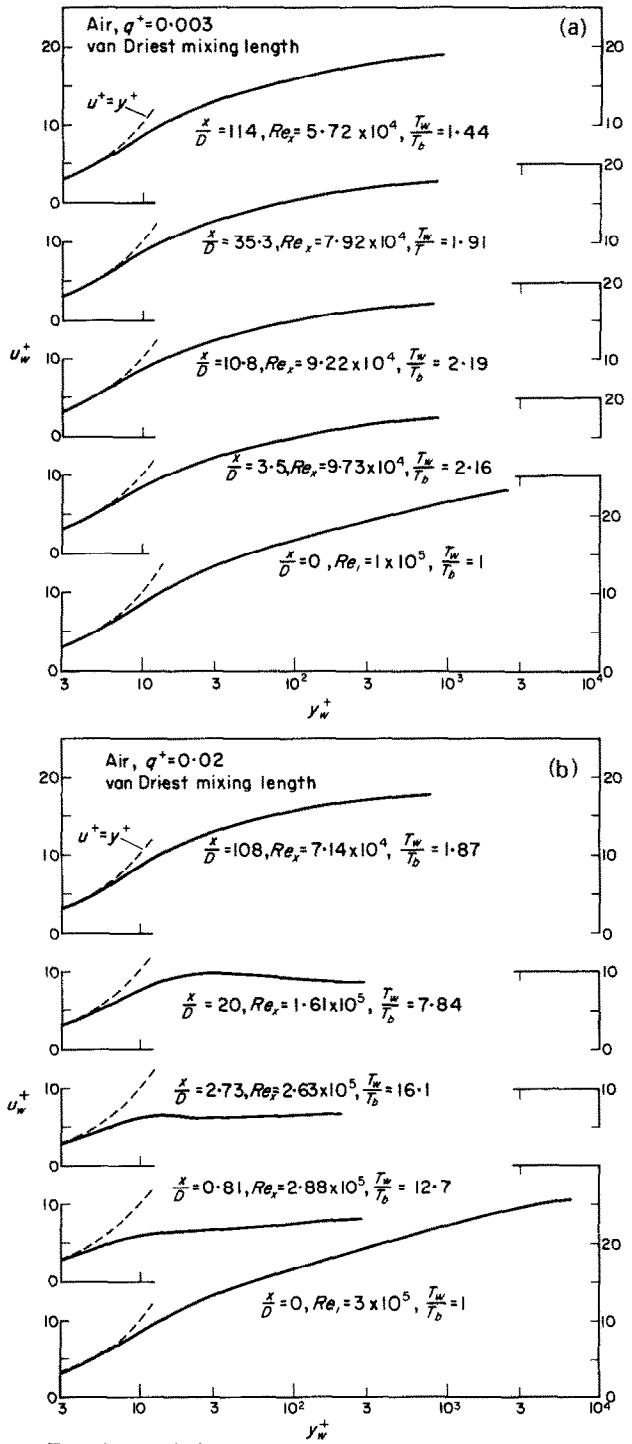

FIG. 10. Turbulent velocity profiles with gas property variation.
(a) Moderate heating rate. (b) Strong heating rates.

laminar-flow results of the present study and of Worsoe-Schmidt and Leppert [8]. In Fig. 10(b), the origins of the maximum may be seen developing as early as 0·8 diameters; by $x/D = 2{\cdot}6$ it is well developed and a minimum occurs closer to the center line. As the flow proceeds downstream the minimum velocity gradually moves to the center line, followed by the maximum (Fig. 11). These locations where the

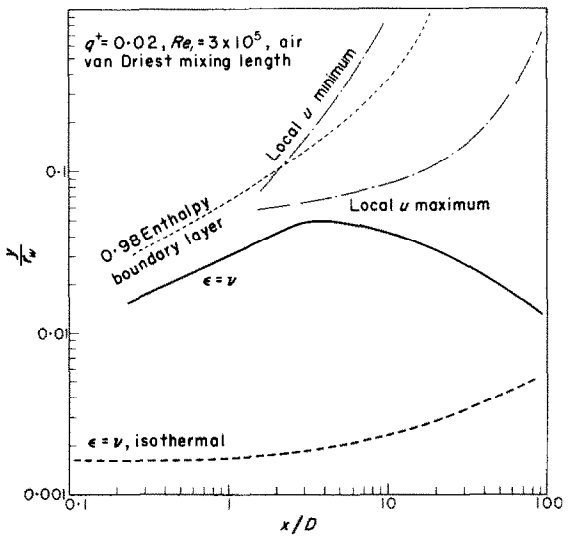

FIG. 11. Axial variation of profile parameters for heated, turbulent flow of air with strong property variation.

velocity gradient becomes zero expose an artificiality of the turbulence model and lead to an anomaly in the temperature profile. With mixing-length models, the total diffusivity reduces to the molecular diffusivity when $(\partial u/\partial y) = 0$; the effective resistance to heat transfer therefore increases locally and the temperature gradient steepens in the vicinity. Thus, from about 2 to 10 diameters, the calculation for $q^+ = 0{\cdot}02$, indicates two transverse locations where ε passes through zero (and $\varepsilon = \nu$ five times), but the temperature gradient is strongly affected only once because the second location is, for the most part, beyond the thermal-boundary layer. The effect is not as serious as it would be for external flow since the heat-transfer coefficient is here defined in terms of bulk temperature rather than of freestream temperature, i.e. center line. Also, when the steep gradient is well established, it is far enough from the wall to have no strong effect on wall behavior. It is of passing interest that others have mentioned separate "core flow" behavior in comparable flows with strongly varying properties [40], but an improved turbulent-flow model is probably needed for such regions rather than the present one.

As noted elsewhere [26], the importance of the pressure drop due to friction diminishes as the heating rate is increased and the pressure drop caused by heating dominates. At low q_i^+, heating reduces f_{app} only slightly. Accordingly, the behavior of the friction factor will be treated only briefly.

Earlier, the utility of the apparent friction factor was emphasized. For the downstream region it is affected slightly less by heating than f_s [26]. In the thermal entry region, f_{app} increases as the heating rate is increased and as x/D is reduced. Consequently, f_{app} varies considerably more than f_s in the first 20–40 diameters, as shown in Fig. 12. The trends in f_{app} correspond

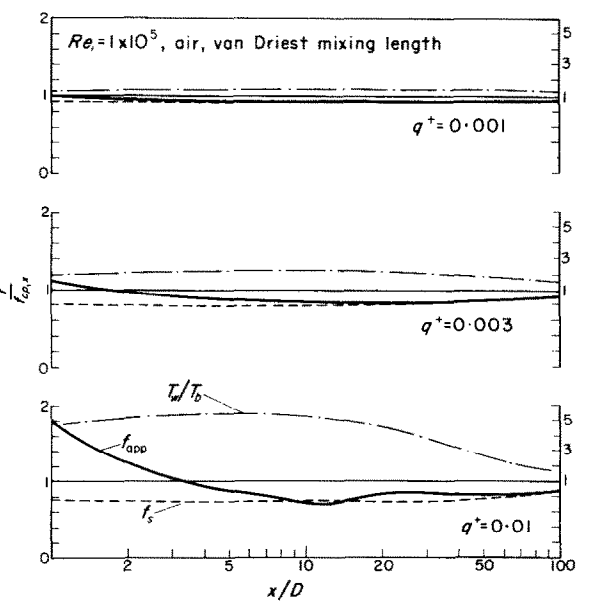

FIG. 12. Wall friction predictions for turbulent flow with property variation. Fully developed entering velocity profile.

to those reported in experiments by McEligot *et al.* [41]. At the lower heating rates, f_{app} is always greater than f_s. However, when the velocity profile becomes severely distorted, as it does at $q^+ = 0{\cdot}01$, f_{app} falls below f_s and then rises above the downstream value as the profile readjusts. This reduction below f_s appears to become greater as the heating conditions become more severe: at $q^+ = 0{\cdot}01$ and $Re_i = 5 \times 10^5$, the minimum in f_{app} is about $f_s/3$, while for the one run at $q^+ = 0{\cdot}02$, f_{app} actually becomes negative. Except for these severe conditions, it appears that the downstream correlation for f_{app} may be used in design without significant error unless the channel length becomes of the order of 10 diameters.

COMPARISON OF PREDICTIONS WITH TURBULENT-FLOW EXPERIMENTS AT HIGH HEATING RATES

The end goal of analysis is prediction. For design problems such as the coolant channels of nuclear reactors, the wall heat flux is known and one wishes to predict surface temperatures and pressure drop. In this section the results of the numerical calculations are compared to data from gas-flow experiments in which the property variation is substantial. Correct prediction of actual temperatures and pressures is taken as the ultimate test of the method.

The calculations in the previous section treated the idealized problem of constant wall heat flux with power-law representations of air properties. For present comparisons the conditions of the experiments are duplicated as well as seemed practicable. The wall heat flux distributions presented in the data are fitted by spline functions. Nitrogen properties derived from NBS-129A and NBS-564 [42, 24] are used,* excepting the compressibility factor in the equation of state which is neglected. For one experiment, which used entering air at room temperature, the power-law properties are retained.

* However, in NBS-129A it is " . . . estimated that in general the tables are accurate within 5 per cent . . ."

Unfortunately, most gas experiments with spectacular property variation have been conducted at relatively low pressure. For example, Taylor lists exit pressures that are only about one-third the entering pressure [2]. Thus, a basic assumption of the analysis is not met in these experiments; $\Delta p/p$ is usually not small enough. Compressibility effects may be expected to become significant above a Mach number about 0·2, but the terms neglected in the governing equations probably do not become important until $M \gtrsim 0{\cdot}4$. The main difficulty with the analysis is the density, which is no longer primarily a function of temperature. Accordingly, the density is computed as a function of both temperature and pressure in most calculations at the experimental conditions, but otherwise the governing equations remain unchanged.

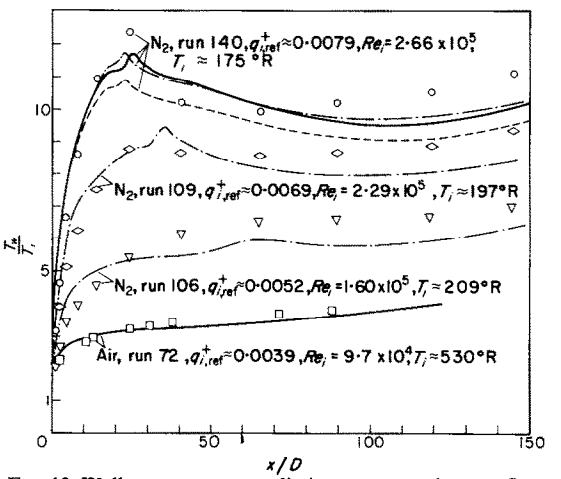

FIG. 13. Wall temperature predictions compared to gas flow experiments with strong heating rates. Runs 106, 109 and 140 from Perkins and Worsoe-Schmidt [1] and run 72 from McEligot *et al.* [41].

Wall temperatures and axial pressure drop are shown compared to several experiments of Perkins and Worsoe-Schmidt [1] and one by McEligot *et al.* [41] in Figs. 13 and 14. All included unheated flow development sections and had approximately constant wall heat flux. The solid lines in the two figures represent

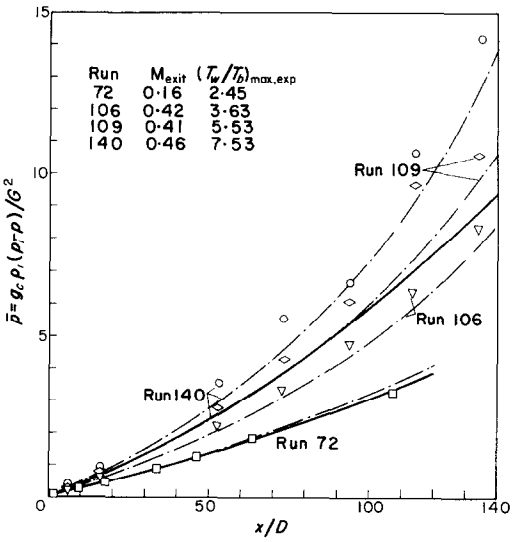

FIG. 14. Pressure drop predictions compared to measurements from gas flow experiments with strong heating.

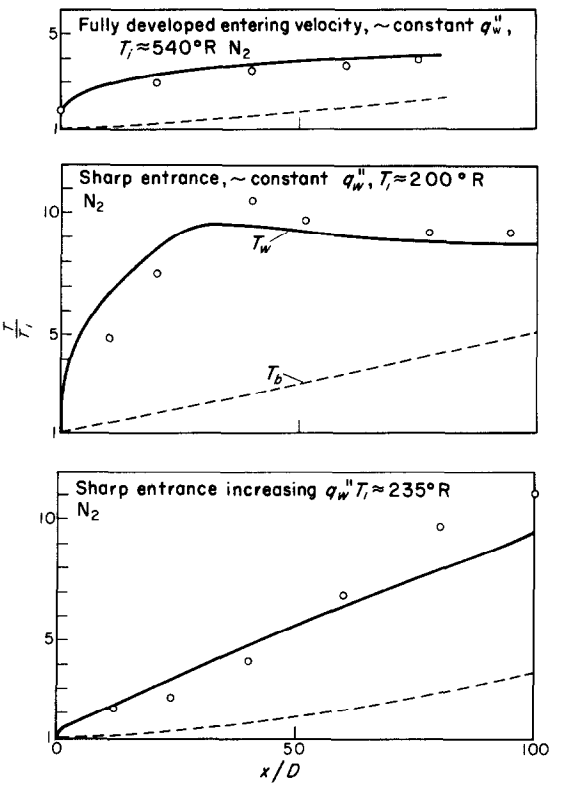

FIG. 15. Comparison between numerical predictions and data of Petukhov *et al.* [43]. Tabulated nitrogen properties [24, 42].

calculations with $\rho = \rho(T)$ while those with "center line" markings were performed with $\rho = \rho(p, T)$. Run 140, used earlier in selecting the turbulence model, is repeated with real nitrogen properties. Shown for comparison, as dashed lines, are the predictions of the earlier section. Revision from power-law air properties to real nitrogen properties yields moderate improvement. On the other hand, there is no major change in wall temperatures when the pressure-dependence in the density is neglected.

The wall-temperature predictions show the same trends as the data: the maximum temperature moves towards the entry as q^+ increases and the peak becomes more abrupt. Consistently, the wall temperature is overpredicted in the entry and underpredicted downstream. One explanation for such a consistent discrepancy lies in the basic use of the turbulence model: The model was originally developed from adiabatic, fully developed flow measurements, hence, the effect in the present treatment is that it is employed on a one-dimensional basis, i.e. only transverse variation is considered in evaluating the mixing length. Physically, we expect some finite distance to be necessary for the upstream turbulence to decay when the viscosity is increasing locally. Thus, in the thermal entry region the analysis predicts the transverse transport to be reduced more rapidly axially, and consequently the predicted wall temperature is higher at a given location.* Further downstream, the temperatures become relatively more uniform across the stream, and the velocity profile, predicted with the one-dimensional turbulent model, therefore approaches its adiabatic form before the turbulence can redevelop from its more damped state. The predicted transport is higher, and wall temperatures consequently are lower than in the laboratory.

* It is recognized that a number of experimental problems could also lead to higher "measured" Nusselt numbers in the thermal entry.

The pressure-drop comparisons are shown in terms of the pressure deficit in Fig. 14. Agreement with run 72 by McEligot *et al.* is good. The requirement for high pressure was met in this test, and the difference between predictions with and without pressure dependence in the equation of state is therefore slight. However, for run 140, with a Mach number of 0·46 at the last pressure tap, the difference in predictions is about 50 per cent at the end of the tube. With the simple modification to the density calculation, agreement with the pressure-drop data of Perkins and Worsoe-Schmidt is fair. In general, the discrepancy seems to be systematic at an approximately constant percentage. Whether the difficulty lies in the simplified analysis—treating only one aspect of the compressibility effects—or in the measurements is unresolved. In calculating $\bar{p}$ from the data, the tube diameter enters to the fourth power and the mass flow rate is squared. A $2\frac{1}{2}$ per cent error in diameter ($\approx$0·003 in) would account for the discrepancy, but a measurement error of this size is unlikely unless there was a change in the surface during operation.

The last figure shows comparison to three interesting experiments by Petukhov *et al.* [43]. Since the parameters of the experiments were determined from minuscule graphs, the uncertainties in describing experimental conditions are possibly somewhat greater than for the other data presented. The first experiment compares to run 72; it has an unheated entrance of forty diameters and approximately constant wall heat flux. The other two utilized an abrupt entrance, one with constant wall heat flux and the other with strongly increasing wall heat flux. Again, the numerical results predict the trends well; agreement (assuming a uniform entering profile) is comparable to that obtained for cases where the experiments and predictions both included flow-development sections. And again, wall temperatures are overpredicted for the entry and underpredicted downstream, even for the increasing heat flux represented in the third subfigure.

Overall, agreement with heat-transfer data for extreme heating is favorable.

SUMMARY

A flexible numerical method has been developed for the solution of coupled equations governing the flow of gases with strongly varying properties through tubes with specified wall heating rates. The method is particularly suited for evaluating hypothesized turbulent-diffusivity models under the stated conditions. In contrast to previous approaches which utilize a specified velocity profile, it is now possible to predict the effects of heating on friction parameters in the thermal entry region by simultaneously solving the momentum and continuity equations along with the energy equation.

Predictions for several proposed turbulent transport models were compared to experimental measurements of surface temperatures at a high heating rate and to data for turbulent flow in the entrance section of a tube. The van Driest mixing-length approach, with wall properties in the exponential term, was found to be operationally the best of the models studied.

Predicted wall temperatures and pressure drops for idealized power-law properties and for real properties showed the trends observed in experiments at strong heating rates. In particular, a local maximum in the wall temperature occurs for heating rates above $q_i^+ = 0{\cdot}005$; it approaches the origin and becomes more abrupt as the heating rate is increased. When based on the version of the van Driest mixing-length model, agreement with the magnitudes of experimental measurements is generally favorable, but not excellent. The need for additional development of turbulence models for application to such strongly heated gas flows is evident.

ACKNOWLEDGEMENTS

The authors appreciate the friendly aid of Professor D. B. Spalding, Imperial College of Science and Technology, London, and of Dr. P. M. Worsoe-Schmidt, Technical University of Denmark, at several stages in this study. Work

at Los Alamos was performed under the auspices of the U.S. Atomic Energy Commission, while work at the University of Arizona was supported by the U.S. Army Research Office, Durham and by an institutional grant from the National Aeronautics and Space Administration. The aid of the Computer Centers at both institutions is acknowledged.

REFERENCES

1. H. C. PERKINS and P. M. WORSOE-SCHMIDT, Turbulent Heat and momentum transfer for gases in a circular tube at wall-to-bulk temperature ratios to seven, *Int. J. Heat Mass Transfer* **8**, 1011–1031 (1965); data tabulated in Tech. Report SU 247–7, Mech. Eng. Dept., Stanford Univ., September (1964).
2. M. F. TAYLOR, Experimental local heat transfer data for precooled hydrogen and helium at surface temperatures up to 5300°R, NASA TN D 2595 (1965).
3. R. SIEGEL, E. M. SPARROW and T. M. HALLMAN, Steady laminar heat transfer in a circular tube with prescribed wall heat flux, *Appl. Scient. Res.* **A7**, 386–391 (1958).
4. E. M. SPARROW, T. M. HALLMAN and R. SIEGEL, Turbulent heat transfer in the thermal entrance region of a pipe with uniform heat flux, *Appl. Scient. Res.* **A7**, 37 (1957).
5. H. C. REYNOLDS, T. B. SWEARINGEN and D. M. McELIGOT, Thermal entry for low Reynolds number turbulent flow, *J. Bas. Engng* **91** (1969).
6. W. M. KAYS, Numerical solutions for laminar-flow heat transfer in circular tubes, *Trans. Am. Soc. Mech. Engrs* **77**, 1265 (1955).
7. H. L. LANGHAAR, Steady flow in the transition length of a straight tube, *Trans. Am. Soc. Mech. Engrs* **64**, A55 (1942).
8. P. M. WORSOE-SCHMIDT and G. LEPPERT, Heat transfer and friction for laminar flow of a gas in a circular tube at high heating rate, *Int. J. Heat Mass Transfer* **8**, 1281–1301 (1965).
9. P. M. WORSOE-SCHMIDT, Heat transfer and friction for laminar flow of helium and carbon dioxide in a circular tube at high heating rate, *Int. J. Heat Mass Transfer* **9**, 1291–1295 (1966).
10. T. B. SWEARINGEN and D. M. McELIGOT, Internal laminar heat transfer with gas property variation (in preparation).
11. R. G. DEISSLER and A. F. PRESLER, Analysis for developing laminar flow and heat transfer in a tube for a gas with variable properties, *Proc. Third Int. Heat Transfer Conf.* Vol. I, pp. 250–256 (1966).
12. R. G. DEISSLER, Analysis of turbulent heat transfer and flow in the entrance regions of smooth passages, NACA TN 3016 (1953).
13. H. WOLF, The experimental and analytical determination of the heat transfer characteristics of air and carbon dioxide in the thermal entrance region of a smooth tube with large temperature differences between the gas and the tube wall, Ph.D. Thesis, Purdue Univ. (1958).
14. W. B. HALL and P. H. PRICE, The effect of longitudinally varying wall heat flux on the heat transfer coefficient for turbulent flow in a pipe, *Int. Developments in Heat Transfer. 2nd Int. Heat Transfer Conf.*, p. 607 (1961).
15. P. M. MAGEE, The effect of large temperature gradients on turbulent flow of gases in the thermal entrance region of tubes, Ph.D. Thesis, Stanford Univ., TID-22247 (1964).
16. P. M. MAGEE and D. M. McELIGOT, Effect of property variation on the turbulent flow of gases in tubes: The thermal entry, *Nucl. Sci. Engng* **31**, 337–341 (1968).
17. R. G. DEISSLER, Analytical and experimental investigation of adiabatic turbulent flow in smooth tubes, NACA TN 2138 (1950).
18. D. B. SPALDING and S. W. CHI, The drag of a compressible turbulent boundary layer on a smooth flat plate with and without heat transfer, *J. Fluid Mech.* **18**, 117 (1964).
19. R. D. RICHTMYER, *Difference Methods for Initial Value Problems*. Interscience, New York (1957).
20. D. GREENSPAN, *Introductory Numerical Analysis of Elliptic Boundary Value Problems*. Harper and Row, New York (1965).
21. J. E. FROMM, A method for computing nonsteady, incompressible, viscous fluid flows, LA-2910, Los Alamos Scientific Laboratory (1963).
22. S. V. PATANKAR and D. B. SPALDING, A finite difference procedure for solving the equations of the two-dimensional boundary layer, *Int. J. Heat Mass Transfer* **10**, 1389–1411 (1967).
23. H. SCHLICHTING, *Boundary Layer Theory*, 4th edn. McGraw-Hill, New York (1960).
24. J. HILSENRATH *et al.*, Tables of thermal properties of gases, NBS Circular 564 (1955).
25. C. A. BANKSTON and D. M. McELIGOT, A numerical method for solving the boundary layer equations for gas flow in circular tubes with heat transfer and property variations, LA-4149, Los Alamos Scientific Laboratory, (1969).
26. D. M. McELIGOT, S. B. SMITH and C. A. BANKSTON, Quasi-developed turbulent pipe flow with heat transfer, to be published in *J. Heat Transfer*.
27. E. R. VAN DRIEST, On turbulent flow near a wall, *J. Aeronaut. Sci.* **23**, 1007–1011 and 1036 (1956).
28. V. L. LEL'CHUK and B. V. DYADYAKIN, Heat transfer from a wall to a turbulent current of air inside a tube and the hydraulic resistance at large temperature differentials, *Problems of Heat Transfer*, AEC-tr-4511, p. 114 (1962).
29. M. F. TAYLOR, Correlation of local heat transfer coefficients for single phase turbulent flow of hydrogen in tubes with temperature ratios to 23, NASA TN D-4332 (1968).
30. H. REICHARDT, Complete representation of turbulent velocity distribution in smooth pipes, *Z. Angew. Math. Mech.* **31**, 208 (1951).
31. H. C. REYNOLDS, M. E. DAVENPORT and D. M. McELIGOT, Velocity profiles and eddy diffusivities for fully developed, turbulent, low Reynolds number pipe flow, *ASME* paper 68-WA/FE-34 (1968).
32. R. M. KENDALL, M. W. RUBESIN, T. J. DAHM and M. R. MENDENHALL, Mass, momentum and heat transfer within a turbulent boundary layer with foreign gas mass transfer at the surface. Part I—constant fluid properties, Vidya Report No. 111, DDC AD 619 209 (1964).

33. P. M. WORSOE-SCHMIDT, Heat transfer in the thermal entrance region of circular tubes and annular passages with fully developed laminar flow, *Int. J. Heat Mass Transfer* **10**, 541–551 (1967).
34. R. W. HORNBECK, An all-numerical method for heat transfer in the inlet of a tube, *ASME* paper 65-WA/HT-36 (1965).
35. M. E. DAVENPORT and G. LEPPERT, The effect of transverse temperature gradients on the heat transfer and friction for laminar flow of gases, *J. Heat Transfer* **87**, 191–196 (1965).
36. P. M. WORSOE-SCHMIDT, Finite difference solution for laminar flow of gas in a tube at a high heating rate, Ph.D. Thesis, Stanford Univ. (1964).
37. A. R. BARBIN and J. B. JONES, Turbulent flow in the inlet region of a smooth pipe, *J. Bas. Engng* **85**, 29–34 (1963).
38. L. M. K. BOELTER, G. YOUNG and H. W. IVERSEN, An investigation of aircraft heaters—XXVII. Distribution of heat transfer rate in the entrance section of a circular tube, NACA TN 1451 (1948).
39. W. M. KAYS, *Convective Heat and Mass Transfer*. McGraw-Hill, New York (1966).
40. K. D. WILLIAMSON, J. R. BARTLIT and R. S. THURSTON, Studies of forced convection heat transfer to cryogenic fluids, *A.I.Ch.E. Sixtieth Annual Meeting, New York* paper 38C, pp. 26–30 (1967).
41. D. M. MCELIGOT, P. M. MAGEE and G. LEPPERT, Effect of large temperature gradients on convective heat transfer: The downstream region, *J. Heat Transfer* **87**, 67–76 (1965).
42. T. R. STROBRIDGE, The thermodynamic properties of nitrogen from 114–540°R between 1·0 and 3000 psia, NBS TN 129A (1963).
43. B. S. PETUKHOV, V. V. KIRILLOV and V. N. MAIDANIK, Heat transfer experimental research for turbulent gas flow in pipes at high temperature difference between wall and bulk fluid temperature, *Proc. Third Int. Heat Transfer Conf.*, Vol. I, pp. 285–292 (1966).

TRANSPORT DE CHALEUR LAMINAIRE ET TURBULENT DANS DES GAZ A PROPRIETES VARIABLES DANS LA REGION D'ENTREE DE CONDUITES CIRCULAIRES

Résumé—On expose une méthode numérique pour résoudre les équations couplées de la couche limite pour l'écoulement turbulent dans un tube circulaire d'un gaz avec de grandes variations de ses propriétés. Des profils de vitesse uniformes et entièrement établis à l'entréé sont pris en considération. La variation axiale de la vitesse d'échauffement est permise et employée pour la comparaison avec les expériences.

Les cas traités sont:

1°) l'écoulement laminaire avec propriétés constantes du fluide et une variation de la longueur d'entrée hydrodynamique;
2°) un profil de vitesse laminaire uniforme à l'entrée avec de l'air à propriétées variable idéalisées;
3°) l'écoulement turbulent entièrement établi avec propriétés constantes au début de la région d'entrée thermique;
4°) l'écoulement turbulent avec propriétés constantes du fluide et un profil de vitesse d'entrée uniforme;
5°) l'écoulement turbulent avec des propriétés variables, idéalisées de l'air et de gaz réél, à des vitesses de chauffage $(q''_w/Gc_{p,i}T_i) = 0{,}02$.

Les prévisions pour plusieurs modèles de transport turbulent sont comparées à une expérience avec un maximum du rapport de température pariétale (T_w/T_i) d'environ 12, et le modèle fournissant l'accord le plus étroit dans la région d'entrée thermique, version du modèle de longueur de mélange de Van Driest, est employé pour des prévisions ultérieures.

TURBULENTER UND LAMINARER WÄRMEÜBERGANG AN GASE MIT VERÄNDERLICHEN STOFFWERTEN IM EINLAUFBEREICH KREISFÖRMIGER KANÄLE.

Zusammenfassung—Es wird eine numerische Methode entwickelt, um die gekoppelten Grenzschicht-gleichungen für turbulente Strömung eines Gases mit stark veränderlichen Stoffeigenschaften in einem Kreisrohr zu lösen. Gleichförmige und voll ausgebildete Eintrittsgeschwindigkeitsprofile werden zugelassen und zum Vergleich mit Experimenten herangezogen.

Die behandelten Fälle schliessen ein (1) konstante Stoffeigenschaften, laminare Strömung mit Variation der hydrodynamischen Einlauflänge; (2) veränderliche idealisierte Stoffeigenschaften für Luft mit gleichmässig laminarem Eintrittsgeschwindigkeitsprofil; (3) konstante Stoffeigenschaften, voll ausgebildete turbulente Strömung im unmittelbaren thermischen Einlaufgebiet; (4) konstante Stoffeigenschaften, turbulente Strömung mit gleichförmigem Eintrittsgeschwindigkeitsprofil; (5) veränderliche idealisierte und reale Stoffeigenschaften für Luft, turbulente Strömung bei Wärmeströmen bis $q''_w/Gc_{p,i}T_i = 0{,}02$.

Berechnungen für mehrere turbulente Transportmodelle werden mit einem Experiment mit einem Grösstemperaturverhältnis (bezogen auf die Wand) T_w/T_i von ungefähr 12 verglichen und das Modell, das die beste Übereinstimmung im thermischen Einlaufgebiet liefert—eine Version von van Driest's Mischungsweg-Modell—wird für weitere Rechnungen benutzt.

ТУРБУЛЕНТНЫЙ И ЛАМИНАРНЫЙ ПЕРЕНОС ТЕПЛА К ГАЗАМ С ПЕРЕМЕННЫМИ СВОЙСТВАМИ ВО ВХОДНОМ УЧАСТКЕ КРУГЛОЙ ТРУБЫ

Аннотация—Разработан численный метод решения взаимносвязанных уравнений турбулентного пограничного слоя газа при значительных изменениях свойств в круглои трубе. Рассматриваются однородные и полностью развитые профили скорости во входной области. Учитываются переменность скорости вдоль оси трубы и приводится сопоставление с экспериментом.

Рассмотренные случаи включают: (1) постоянные свойства жидкости, ламинарное течение при изменении длины гидродинамического входного участка; (2) переменные идеализированные свойства воздуха при однородном профиле скорости в ламинарной входной области; (3) постоянные свойства, полностью развитое турбулентное течение на участке тепловой стабилизации; (4) постоянные свойства жидкости, турбулентное течение, при однородном профиле скорости во входной области; (5) переменные, идеализированные свойства воздуха и свойства реального газа, турбулентный поток при скоростях потока до $(q''_w/GC_{p,i}T_i) = 0.02$.

Расчеты нескольких турбулентных моделей переноса сравниваются с экспериментом прм отношении максимальной температуры стенки $T_w/T_i = 12$. Модель указывает на хорошее соответствие в термической входной области. В дальнейших расчетах используется вариант модели Ван Дриста для пути перемешивания.